Lateral Organization of Liquid-Crystalline Cholesterol−Dimyristoylphosphatidylcholine Bilayers. Evidence for Domains with Hexagonal and Centered Rectangular Cholesterol Superlattices†

Jorma A. Virtanen,‡ Mika Ruonala,§ Matti Vauhkonen,§ and Pentti Somerharju*,§

Institute of Biomedicine, Department of Medical Chemistry, University of Helsinki, Helsinki, Finland, and Department of Chemistry, University of California at Irvine, Irvine, California

Received March 2, 1995; Revised Manuscript Received June 26, 1995⊗

ABSTRACT: The lateral organization of fluid cholesterol−dimyristoylphosphatidylcholine (DMPC) bilayers was studied by measuring the response of fluorescent membrane probes, dipyrenylphosphatidylcholines (diPyr$_x$PCs) or merocyanine 540, to the variation of cholesterol concentration. Parallel absorbance and light-scattering measurements were also carried out. The excimer-to-monomer ratio of diPyr$_x$PCs displayed abrupt deviations at particular cholesterol mole fractions (CMFs). The most notable of these occurred at CMFs of 0.15, 0.33, and 0.67. Deviations were also frequently observed at CMFs of 0.12, 0.20, 0.25, and 0.40. Merocyanine 540 reproducibly reported deviations at CMFs of 0.15 and 0.33 and frequently reported values close to 0.12, 0.20, and 0.25. In absorbance (turbidity) and light scattering versus CMF plots, well-defined kinks were observed at CMFs of 0.16, 0.33, 0.52, and 0.67. The occurrence of kinks or other deviations at those particular CMFs is most readily explained in terms of a superlattice model previously developed to explain the lateral distribution of pyrenylphospholipids in bilayers [Somerharju, et al. (1985) *Biochemistry 24*, 2773−2781; Virtanen, J. A., et al. (1988) *J. Mol. Electron. 4*, 233−236]. This model is based on the assumptions that (i) each cholesterol molecule replaces a single acyl chain in a hexagonal lattice, (ii) cholesterol molecules, because of their larger size, perturb the lattice, (iii) this perturbation is minimized when the cholesterol molecules are maximally separated from each other, and (iv) the maximal separation is achieved when the cholesterol molecules form a hexagonal or centered rectangular superlattice. All detected critical CMFs, except that at CMF 0.67, are predicted by the model, thus strongly supporting its validity. The critical CMF at 0.67 is a limiting case, which can be accounted for by assuming that cholesterol and phospholipid molecules form alternating rows, i.e., formation of a cholesterol superlattice with rectangular symmetry. As predicted by the superlattice model, composition-driven order-to-disorder transitions occur between the critical CMFs, as indicated by increased data scatter and sample fluctuations in those regions. Another important prediction of the superlattice model is that domains with different cholesterol superlattices should coexist at most cholesterol concentrations. Such domains do not have to be extensive to account for the critical events observed here; rather, they are expected to be dynamic entities of limited size. It is very likely that such microscopic domains with distinct cholesterol superlattices also coexist in biological membranes. This is expected to have remarkable effects on both the structure and functions of these membranes.

Cholesterol is a major component of membranes and is indispensable for mammalian cells (Yeagle, 1993; Bloch, 1988). However, despite numerous biophysical, biochemical, and cell biological studies, the critical function(s) of cholesterol has not been firmly established. Experiments with model membranes have shown that cholesterol dramatically reduces the permeability of phospholipid bilayers to polar solutes (Blok et al., 1977). This, together with the enrichment of cholesterol to the plasma membrane (Lange et al., 1989), indicates that cholesterol plays an important role in the regulation of the permeability of the cell membrane. Cholesterol markedly enhances the orientational order and, consequently, the packing of lipid acyl chains (Seelig & Seelig, 1980; Vist & Davis, 1990; Sankaram & Thompson, 1990). Thus, cholesterol could also serve to make the membranes, the plasma membrane in particular, more resistant to mechanical stress (Yeagle, 1985). There is experimental and theoretical evidence that the addition of cholesterol to phospholipid bilayers can lead to the separation of immiscible fluid phases or domains with distinct cholesterol concentrations (Lenz et al., 1980; Rectenwald & McConnell, 1981; Ipsen et al., 1987; Vist & Davis, 1990; Sankaram & Thompson, 1990, 1991). Such fluid−fluid immiscibility could play an important role in various membrane-related phenomena, including protein and lipid sorting (Bretscher & Munro, 1993).

The physical principles responsible for cholesterol-induced phase separation or domain formation are not well-established, and several alternative models have been put forward. Cholesterol−phospholipid complexes, involving

† This work was supported by grants from the Finnish Academy and Sigrid Juselius Foundation to P.S. and the Finnish Cultural Foundation to J. V.

* Address correspondence to this author at Institute of Biomedicine, Department of Medical Chemistry, P.O. Box 8, 00014 University of Helsinki, Helsinki, Finland; Fax 358-1918276, E-mail Somerharju@Katk.Helsinki.Fi.

‡ University of California at Irvine.

§ University of Helsinki.

⊗ Abstract published in *Advance ACS Abstracts,* August 15, 1995.

0006-2960/95/0434-11568$09.00/0

hydrogen bonding at the head-group level, with 1/1 or 1/2 stoichiometry have been proposed to be instrumental in such phase separations (Presti et al., 1982). Related to this model, the formation of (two-dimensional) compounds with different cholesterol/phospholipid stoichiometries has been suggested (Rubenstein et al., 1980; Lundberg, 1982). Alternatively, the addition of cholesterol may induce a population of phospholipids with conformationally ordered acyl chains, and this population forms segregated domains in a matrix of conformationally disordered phospholipid molecules (Ipsen et al., 1987).

Previously, we and others have found that when increasing amounts of a pyrenylacyl-PC (PyrPC)[1] were added to liquid-crystalline phosphatidylcholine bilayers, the excimer-to-monomer fluorescence intensity ratio (*E/M*) versus PyrPC mole fraction plots display several "kinks" or "dips" that occur at particular (critical) PyrPC mole fractions (Somerharju et al., 1985; Tang & Chong, 1992; Chong et al., 1994). These critical mole fractions could be explained in terms of a simple geometrical model based on the assumptions that (i) the bulky pyrenyl moieties create local packing defects, and (ii) to minimize the energy due to these defects, the pyrenyl acyls tend to separate maximally. In a hexagonal host (acyl chain) lattice, such a maximal (and equal) separation of the PyrPC molecules would result in the formation of pyrenylacyl superlattices with a hexagonal symmetry. According to the model, the kinks or dips observed at the particular PyrPC mole fractions correspond to the situation where domains with a particular superlattice prevail, while at the intermediate concentration regimens, domains with distinct superlattices would coexist (Somerharju et al., 1985; Virtanen et al., 1988; Tang & Chong, 1991). The model also allows for the presence of areas or domains with a random distribution of the components coexisting with those having a regular, superlattice-like organization (Sugar et al., 1994).

Since cholesterol, like a pyrenylacyl chain, contains a rigid and bulky ring system, it seemed possible that cholesterol could also form domains with a particular stoichiometry and arrangement of the components. To test this, we have monitored the physical properties of DMPC−cholesterol liposomes as a function of cholesterol concentration by using the fluorescent probes diPyr$_x$PCs and merocyanine 540 (MC540), as well as absorbance measurements. The results show that at certain (critical) cholesterol mole fractions (CMFs) the physical properties of the bilayer change abruptly. These critical CMFs coincide closely with those predicted by a superlattice model, thus supporting the existence of domains with cholesterol superlattices in DMPC−cholesterol bilayers.

EXPERIMENTAL PROCEDURES

Chemicals. Dimyristoyl-*sn*-3-glycerophosphocholine (DMPC) was purchased from Avanti Polar Lipids (Alabaster, AL) and cholesterol (99+% grade) was from Sigma (Deisenhofen, Germany). Dipyrenylacyl-*sn*-3-glycerophosphocholines (diPyr$_x$PCs) were synthesized using previously described methods (Somerharju et al., 1985). Stock solutions of the lipids were prepared in chloroform and stored in the dark at −25 °C. Merocyanine 540 was from Molecular Probes (Eugene, OR). HPLC-quality solvents were obtained from Merck (Espoo, Finland), and all other chemicals were from Sigma. The concentration of cholesterol was determined gravimetrically, and that of DMPC was determined according to Rouser et al. (1970). The concentrations of diPyr$_x$PCs were determined by absorbance measurements in ethanol using 84 000 cm^{-1} as the molar extinction coefficient (Somerharju et al., 1985).

Preparation of DMPC−Cholesterol Stock Mixtures and Lipid Dispersions. From a DMPC stock solution (30 mM in chloroform), a constant volume was pipetted into small screw-cap vials with a microsyringe equipped with a Chaney adapter. Then the appropriate amount of cholesterol (10 mM in chloroform) was similarly added to obtain the desired cholesterol mole fraction. After thorough mixing these DMPC−cholesterol stock mixtures were stored in the dark at −25 °C. From these stock mixtures, 100 μL (corresponding to 100 nmol of DMPC) was transferred to solvent-cleaned glass tubes containing 200 μL of chloroform with a microsyringe. After addition of the diPyr$_x$PC probe (0.2−0.3 mol%) and thorough mixing, the samples were placed in a 45 °C water bath and the solvent was evaporated under a stream of nitrogen by using a manifold with a capacity of 100 tubes. The samples were then kept under oil pump vacuum for >2 h to remove any residual solvent. This time period was chosen because extension of the evacuation period to 7 h did not have any detectable effect on the results. After the tubes were filled with argon, 2 mL of prewarmed (40 °C) TEN buffer (20 mM Tris-HCl, 1 mM of EDTA, and 150 M NaCl, pH 7.4) was added and the tubes were transferred into a 40 °C water bath for >15 min, after which the lipids were dispersed by brief (20 s) sonication (55 W output) using a Branson sonifier equipped with a microtip. The tubes were then placed in a 31 °C water bath for 2 h before measurement in order to equilibrate the samples with air. Merocyanine 540 was added to preformed lipid dispersions that were then incubated for 1 h at 30 °C before measurement. In some experiments the sonication period was shortened to 10 s, and three heating/cooling cycles (30 min at 38 °C/30 min at 2 °C) were performed before the measurement. We dispersed the lipid by brief sonication rather than by vortex mixing because the coarse dispersions produced by the latter method resulted in an unacceptably unstable signal in our fluorometer, obviously due to fluctuations in the number of liposomes in the excitation beam.

We preferred to dry the lipid mixtures from chloroform because it was previously observed that drying of DMPC−cholesterol mixtures from this solvent produces apparently homogeneous particles, while drying from methanol produces heterogeneous ones (Rubenstein et al., 1980). It has also been shown that less cholesterol is incorporated into phospholipid vesicles if the lipid mixture is dried down from an alcohol (ethanol) instead of from chloroform (Freeman & Finean, 1975). The relatively high evaporation temperature (45 °C) used here should also assist in producing homogeneous dispersions.

[1] Abbreviations: CMF, cholesterol mole fraction; CR, centered rectangular; DHE, dehydroergosterol; DMPC, dimyristoylphosphatidylcholine; diPyr$_x$PC, dipyrenylacylphosphatidylcholines, *x* indicates the length of the acyl chains; EDTA, ethylenediaminetetraacetic acid; *E/M*, excimer to monomer fluorescence intensity ratio; egg PC, egg-yolk phosphatidylcholine; HPLC, high-performance liquid chromatography; HX, hexagonal; MC540, merocyanine 540; PC, phosphatidylcholine; PyrPC, 1-palmitoyl-2-pyrenylacylphosphatidylcholine; SD, standard deviation; SL model, superlattice model; TEN, Tris−EDTA−NaCl buffer; T_m, gel-to-liquid transition temperature.

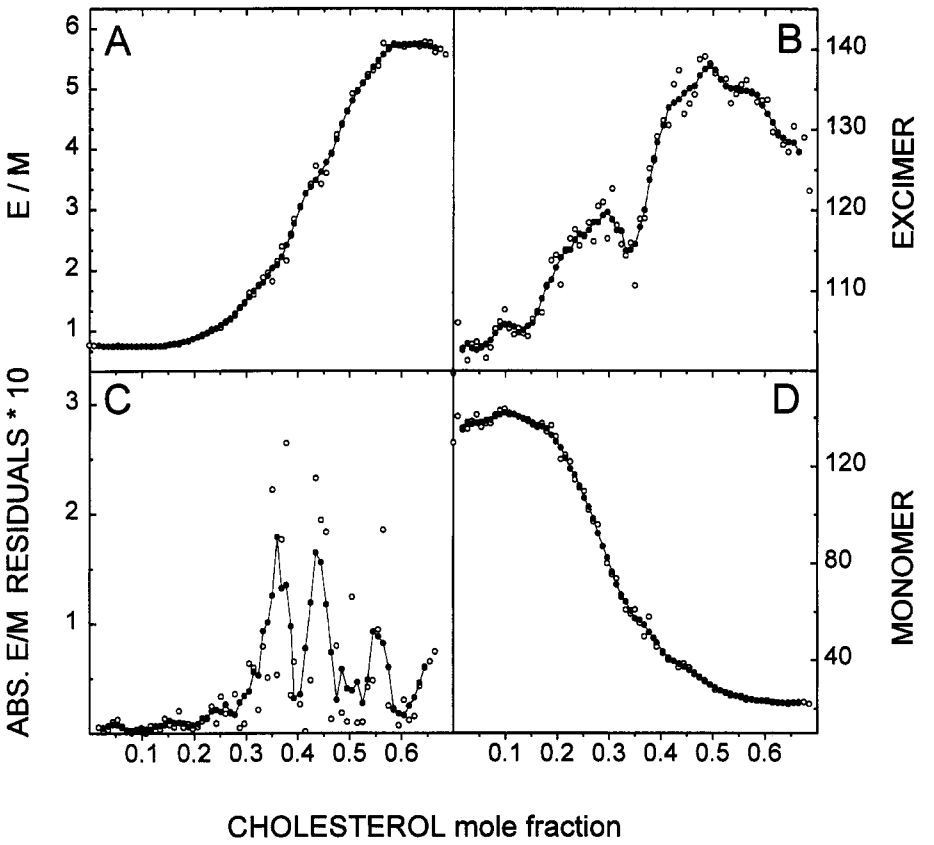

FIGURE 1: Effect of bilayer cholesterol concentration on the fluorescence parameters of diPyr$_{12}$PC in DMPC liposomes. *E/M*, the excimer-to-monomer intensity ratio (A), the excimer intensity (B), and the monomer intensity (D) are plotted against cholesterol mole fraction. The open symbols are the measured data points, while the closed symbols represent data smoothed using a five-point running average. Note that while smoothing helps to show general trends, it also tends to moderate or even obscure deviations determined by few data points only. In panel C, absolute residuals between the measured values of *E/M* and the smoothed data are plotted versus cholesterol mole fraction as an indicator of local data scatter (see Experimental Procedures). Very similar plots were obtained when diPyr$_{14}$PC was used as the probe (not shown).

Fluorescence, Absorbance, and Light-Scattering Measurements. After equilibration, the samples were transferred to a quartz cuvette and placed in the thermostated cuvette holder of a Hitachi F-4000 fluorescence spectrophotometer, and the intensity was measured at 378 (monomer) and 475 nm (excimer) for the samples containing a dipyrenyl lipid or at 560 and 590 nm when merocyanine was used as the probe. The excitation wavelengths were 344 and 540 nm for the dipyrenyl probes and MC540, respectively. The temperature of the samples was 29.6−29.7 °C at the time of measurement as monitored with a thermocouple probe.

Light scattering at the 90° angle was measured with the fluorescence spectrophotometer by adjusting both the excitation and emission monochromators to either 378 or 475 nm. The absorbances (turbidity) at 378 and 475 nm were measured with a Perkin-Elmer 550 SE spectrophotometer at 30 °C.

Data Analysis. In the fluorescence experiments, three readings were taken approximately 4 s apart at each wavelength, and the average was calculated and plotted against CMF. In the absorbance measurements only a single reading was taken using a 5 s integration time. Since the deviations (kinks or dips) in the measured parameter versus CMF plots frequently were rather small and/or tended to be obscured by (locally) increased data scatter, data averaging and/or running average smoothing were used to detect the significant deviations. An unavoidable drawback of the running average method is that deviations defined with only a few data points are moderated considerably . Generally, the significance of a deviation was estimated by comparing its magnitude to the average scatter of the smoothed data, as well as by the reproducibility of its occurrence. We also attempted to estimate the significance of the deviations by determining the standard deviations of data averaged from several parallel experiments. This was, however, problematic due to small (uncontrollable) variations in (i) sample dispersion procedure, (ii) sample volume due to evaporation during sample equilibration, (iii) measurement temperature, and (iv) sample oxygen concentration. The pyrene fluorescence intensities are particularly sensitive to the last parameter due to the long excited state lifetime.

Data scatter was analyzed by plotting either standard deviations between three consecutive data points (which was considered approximately equal to determining the standard deviation between three parallel data points because of the small cholesterol concentration intervals used) or the residuals between the smoothed curve (obtained by using a 3−5 point running average) and the individual data points. We realized that artificial scatter peaks or other kinds of distortions in the profiles may be generated when there is an abrupt change (dip or kink) in the measured parameter versus CMF plot. In the case of SD plots, this happens because the (true) values of three consecutive points can be considerably different in regions where an abrupt change occurs; thus, the SD is increased although there is no true increase in the data scatter proper. In case of the residual

plots, the distortion arises from the (intrinsic) inability of a smoothed curve to accurately follow any abrupt changes in the plot. However, it is relatively straightforward to distinguish between true and artificial scatter peaks (or minima) by comparing the scatter profiles with the measured parameter versus CMF plots.

The (time-dependent) fluctuation in sample fluorescence intensity was estimated by plotting the SD of three consecutive readings recorded with an approximate time interval of 4 s. Again, averaging of data from parallel experiments and running average smoothing was used to reveal the general trends.

RESULTS

Dipyr$_x$PCs as Probes for DMPC−Cholesterol Lateral Mixing. The formation of intramolecular excimers by long-chain diPyr$_x$PC markedly increases with cholesterol content in liquid phosphatidylcholine bilayers (Eklund et al., 1992), suggesting that such lipids could be useful to study the modulation of the physical properties of phospholipid bilayers by cholesterol. This increased excimer formation very likely results from conformational ordering of the acyl chains by the rigid body of cholesterol (Mendelsohn et al., 1991), which brings the two pyrenyl residues of long-chain diPyr$_x$-PC closer together with a consequent increase in intramolecular excimer formation. Supporting this, we have recently shown that cholesterol markedly decreases the width of the transversal distribution of acyl-bound pyrenyl moieties (Eklund et al., 1992; Sassaroli et al., 1995). Furthermore, cholesterol does not increase the excimer formation of short-chain diPyr$_x$PCs (see the following), obviously because the pyrenyl moieties attached to short, conformationally restrained acyl chains are bound to stay proximal to each other even in the absence of cholesterol.

Accordingly, DMPC liposomes containing a variable amount of cholesterol and a trace amount (0.2−0.3 mol%) of a diPyr$_x$PC probe were prepared and subjected to *E/M* determination. As depicted in Figure 1A, *E/M* determined for diPyr$_{12}$PC-labeled liposomes increased by about 10-fold when the cholesterol mole fraction (CMF) increased from 0 to 0.70. The increase leveled off around CMF 0.60 and started to decline above CMF 0.65−0.66. Interestingly, deviations also seem to occur at lower CMFs in the *E/M* plot, most notably around 0.33−0.40, indicating that critical events may take place in those regions. That this is indeed the case is demonstrated by Figures 1B,C, where excimer and monomer intensities are plotted versus CMF for diPyr$_{12}$-PC. The excimer curve shows marked deviations (dips) at CMFs 0.12−0.16 and 0.34, while in the monomer curve kinks or deviations are seen at CMFs 0.11−0.12, 0.33, and probably also close to 0.20 and 0.40. Practically identical results were obtained when diPyr$_{14}$PC was the probe (not shown). The presence of such deviations strongly suggests that critical mixing events take place at the respective CMFs. To study this further, more limited CMF intervals were examined. Figure 2 displays the *E/M* of diPyr$_{10}$PC for CMF 0−0.20. Clear kinks are observed close to CMFs 0.11−0.12 and 0.15−0.16. A kink at the latter CMF was observed reproducibly by using different cholesterol−DMPC stock solutions (not shown) and is thus considered to be a significant one (see also Figure 1B). While a kink was also seen close to CMF 0.12 in most experiments, it could not be unambiguously detected in some, possibly because it was obscured by the increased data scatter typically occurring close to this and other kinks or dips (see below).

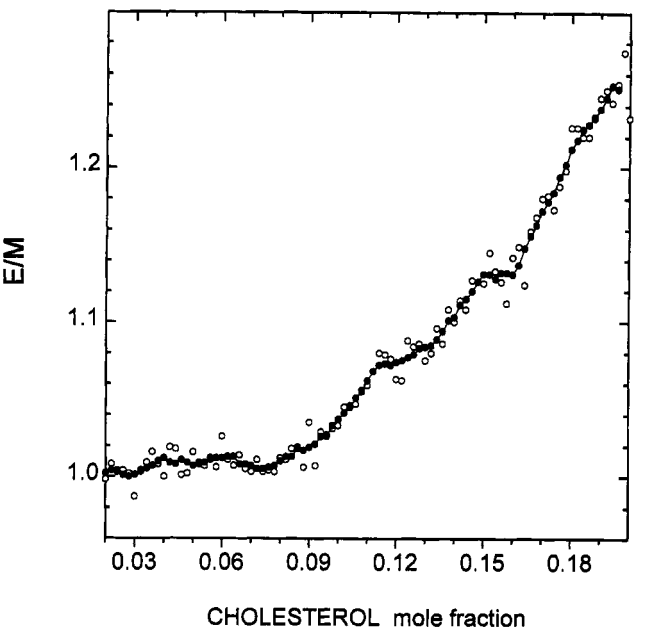

FIGURE 2: Excimer-to-monomer ratio of diPyr$_{10}$PC versus cholesterol mole fraction in DMPC liposomes. The open symbols represent averages from two parallel experiments, and the closed symbols represent the data smoothed using a five-point running average. The kink seen close to CMF 0.15 was observed constantly and that at CMF 0.12 was observed frequently with samples prepared from different DMPC−cholesterol stock solutions. Note the increased data scatter between these two CMFs.

Figure 3A displays the *E/M* plot for the CMF region 0.40−0.80 obtained with diPyr$_{10}$PC as the probe. The change in *E/M* leveled off at CMF 0.65−0.67 in accordance with the data obtained with DiPyr$_{12}$PC as the probe (Figure 1A,C). Critical events may also take place close to CMF 0.50, as indicated by increased data scatter in this region (see the following). When the short-chain derivatives, diPyr$_4$PC and diPyr$_6$PC, were employed, *E/M* decreased rather than increased with cholesterol concentration, in line with our earlier findings (Eklund et al., 1992). However, with these probes, saturation of the change (decrease) in *E/M* also occurred close to CMF 0.64−0.67 (not shown).

A kink at or very close to CMF 0.20 was observed in nearly all *E/M* versus CMF plots obtained with different cholesterol−DMPC stock solutions and/or other diPyr$_x$PC probes (not shown). Generally, this kink was not as pronounced as those seen close to CMFs 0.12 and 0.15. However, the critical nature of CMF is supported by other data discussed here. In some, but not all, experiments deviations were also observed close to CMFs 0.40 and 0.50. Interestingly, a markedly increased scatter of the data appeared to occur close to those CMFs where deviations were observed. To examine this further, two simple methods of scatter analysis were employed (see Experimental Procedures for their details and limitations). They consisted of plotting either the standard deviations of three sequential data points or the residuals between the smoothed and measured data against CMF. Figure 1C shows a plot of residuals for the *E/M* data of Figure 1A. Several peaks of data scatter with minima close to CMFs 0.20, 0.33, 0.40, and 0.50 are present. The statistical significance of these scatter peaks is supported

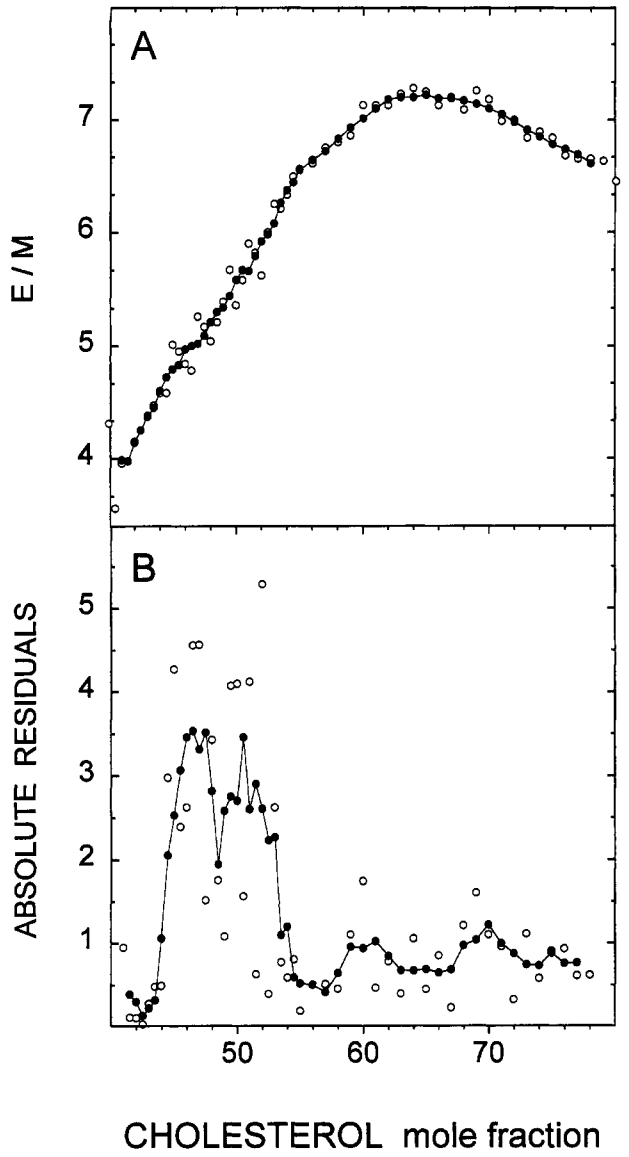

FIGURE 3: Effect of bilayer cholesterol concentration on the fluorescence parameters of diPyr$_{10}$PC in DMPC liposomes: (A) ratio of excimer-to-monomer fluorescence intensity versus cholesterol mole fraction (symbols as in Figure 1); (B) absolute *E/M* residuals versus cholesterol mole fraction. Open and closed symbols represent the raw data and the data smoothed using a five-point running average, respectively. The data are from a single experiment. Consistent results were, however, obtained in several other experiments where other DMPC–cholesterol stock solutions (with different data point intervals) and/or other diPyr$_x$PC probes were used.

by the finding that the data averaged from four parallel experiments (Figure 4) retain the essential features of that shown in Figure 1D. Highly increased data scatter close to CMF 0.50 is also seen in Figure 3B.

Plots covering lower CMF regions frequently showed scatter peaks close to CMFs 0.12 and 0.15 (not shown). While the lack of complete reproducibility of the scatter profiles might suggest that the observed scatter peaks or minima are not statistically significant, it should be noted that highly reproducible profiles are not to be expected because data scatter is a stochastic phenomenon, and because of the relatively small number of data points defining each peak or minimum. In addition, the closeness of certain critical CMFs (cf. Table 1), and thus their associated scatter peaks, is also likely to contribute to such variability. Aside

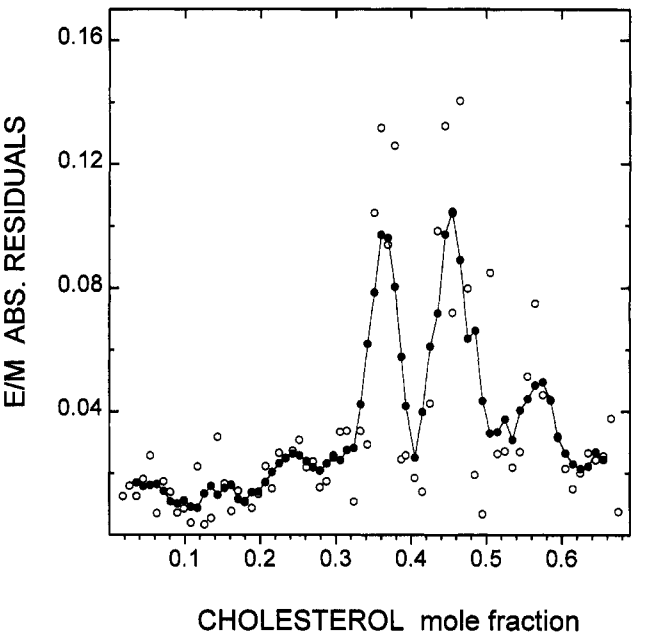

FIGURE 4: Scatter of the fluorescence data versus cholesterol mole fraction. As an approximate measure of data scatter, the absolute *E/M* residuals together with the five-point running average are plotted against cholesterol mole fraction. Data from three parallel experiments were averaged. See Experimental Procedures for the details of data analysis. An abrupt increase in data scatter occurs close to CMFs 0.33, 0.40, and 0.50. Consistent results were obtained with other DMPC–cholesterol stock solutions and/or diPyr$_x$PC probes.

Table 1: Critical Cholesterol Mole Fraction Corresponding to Hexagonal or Centered Rectangular Superlattices as Predicted by the Superlattice Mode

a[b]	b[b]	*hexagonal*[a]	*centered rectangular*[a]
1	1	0.50	0.50
0	2	0.40	0.40
2	1	0.25	*0.333*[c]
1	2	0.25	0.222
0	3	0.20	0.20
2	2	0.154	0.154
1	3	0.143	*0.125*
0	4	0.118	0.118
2	3	0.10	0.091
1	4	0.091	*0.08*
3	3	0.071	0.071

[a] The critical CMFs corresponding to hexagonal and centered rectangular symmetries were obtained according to eqs 1 and 2, respectively, with $f = 1$ (see text). Note when $a = 0$ or $a = b$, the same critical CMFs are given by eqs 1 and 2. [b] a and b are the cholesterol superlattice coordinates as defined in Virtanen et al. (1988) and Tang and Chong (1992). [c] The critical CMFs unique to the centered rectangular symmetry have been italicized.

from such experimental uncertainties, critical events could occur at CMFs somewhat different from the predicted ones because of transbilayer asymmetry. The bilayers of sonicated liposomes used here may have significant curvature, and thus lipid packing may be different in the inner and outer leaflets of the bilayer due to their opposite curvatures. Because of geometrical constraints, cholesterol may be unevenly distributed between the two leaflets, particularly at high cholesterol concentrations, as indicated by the data of Huang et al. (1974). If so, critical events would occur at overall cholesterol concentrations that are different from those predicted by assuming symmetric distribution. The occur-

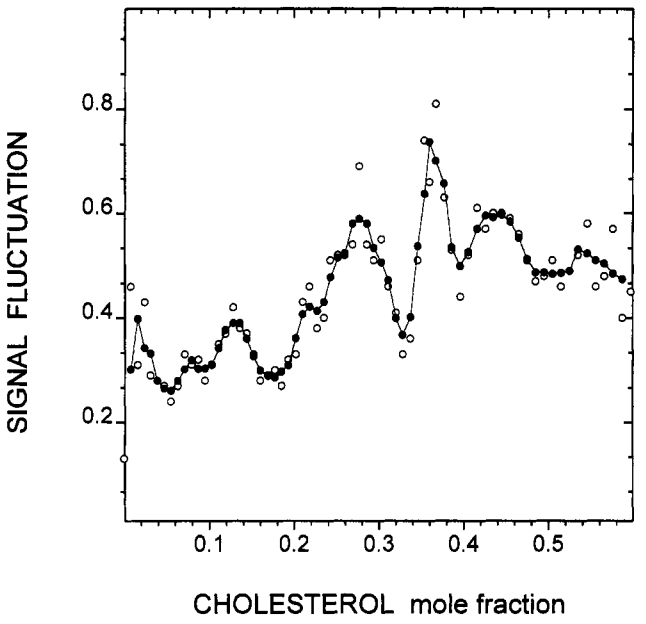

FIGURE 5: Fluctuation in the fluorescence intensity as a function of cholesterol mole fraction. The time-dependent fluctuation of the sample excimer intensity in the cuvette was determined as described under Experimental Procedures. Data (open symbols) from five parallel experiments were averaged. The smoothed data (three-point running average, closed symbols) are also shown to indicate the general trends.

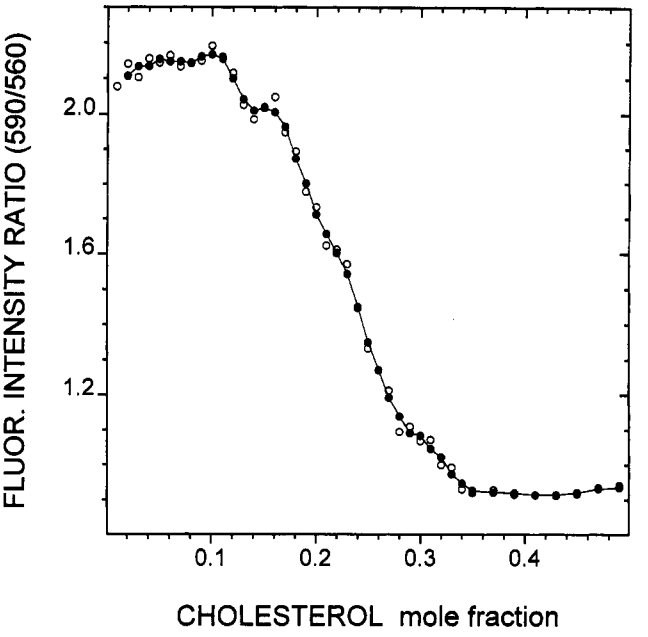

FIGURE 6: Binding of merocyanine 540 to DMPC–cholesterol liposomes as a function of cholesterol mole fraction. The ratio of fluorescence intensities at 590 and 560 nm is plotted as an indicator of the amount of merocyanine bound to the liposomes (see Experimental Procedures). Open symbols represent data averaged from five parallel experiments, and the closed ones represent three-point running averages. Marked deviations are seen close to CMFs 0.12, 0.15, 0.2, and 0.34. Consistent results were obtained with samples prepared from other DMPC–cholesterol stock mixtures having different cholesterol concentration intervals.

rence of minima or kinks at CMF 0.55–0.60 (Figures 1C, 3B, and 8) especially could result from the asymmetric distribution of cholesterol.

As an additional test for critical CMFs, the standard deviations of three consecutive readings of fluorescence intensity were determined. Figure 5 displays such a "sample fluctuation" plot for the excimer intensity, averaged from five parallel experiments, for the CMF region 0.05–0.60. Minima appear to be present at CMFs 0.15/0.20, 0.33, 0.40, and 0.50. There are also indications of a possible minimum close to 0.25.

As will be discussed in the following, both the time-dependent intensity fluctuations as well as the data scatter probably correlate with the heterogeneity of the liposomes, which in turn depends on the lateral homogeneity of the lipid bilayers upon dispersion of the lipids. Thus, these results indicate that the lateral homogeneity of DMPC–cholesterol bilayers is maximal at the CMFs where scatter and fluctuation minima are observed (see Discussion).

Merocyanine 540 Binding versus Cholesterol Mole Fraction. Binding of merocyanine 540 (MC540) to membranes is known to be sensitive to cholesterol-induced changes in lipid packing (Williamson et al., 1983; Humphries & Lovejoy, 1983). Therefore, we also investigated whether critical CMFs would be detectable by measuring MC540 binding to the liposomal membranes. The binding of MC540 was generally determined from the ratio of the fluorescence intensities at 590 and 560 nm, which correspond to the emission maxima of membrane-bound and free MC540, respectively (Verkman, 1987). In addition, 590 nm intensity plots were used to detect critical CMF.

Typical binding data are shown in Figure 6. Clearly, the binding of MC540 is strongly dependent on the amount of cholesterol in the bilayer, as was found previously (Williamson et al., 1983; Humphries & Lovejoy, 1983). More importantly, however, several kinks and deviations are observable. The most notable of these occurs at a CMF of 0.33–0.34, where the 590/560 intensity ratio levels off abruptly, probably because MC540 cannot bind to the membrane beyond this CMF. Discontinuities also appear to occur close to CMFs 0.12, 0.16, and 0.20/0.25. The discontinuities close to 0.12 and 0.25 are more clearly shown by another set of experiments (Figure 7). In this case a higher data point density was used, and the intensity at 590 nm was plotted instead of the 590/560 ratio. It is to be noted that the general shape of the fluorescence intensity (at 590 or 560 nm) and the 590/560 ratio versus CMF plots was dependent on the amount of MC540 used (not shown). This is probably due to concentration-dependent formation of nonfluorescent MC540 dimers in the bilayer (Verkman, 1987). However, despite this variability, the abrupt deviations were consistently observed at the same CMFs, i.e., close to 0.12, 0.15, 0.20, 0.25, and 0.33. Analysis of data scatter showed that scatter peaks close to these CMFs were frequently present (not shown), in agreement with the diPyr$_x$-PC data.

Absorbance and Light-Scattering Measurements. Since absorbance and light scattering of liposomes are sensitive to the physical state of the bilayer (Yi & MacDonald, 1973), we carried out such measurements on DMPC liposomes containing variable amounts of cholesterol. In Figure 8 the absorbance is plotted for the CMF region 0–0.66. Well-defined kinks are observed at 0.15–0.16, 0.34, and 0.52. In addition, the data are consistent with the occurrence of kinks at 0.20 and 0.07–0.08. Figure 9 displays the absorbance for CMF 0.40–0.75. An abrupt increase is observed at 0.66–0.67. Light-scattering measurements gave very similar results (not shown). The abrupt increase in absorbance

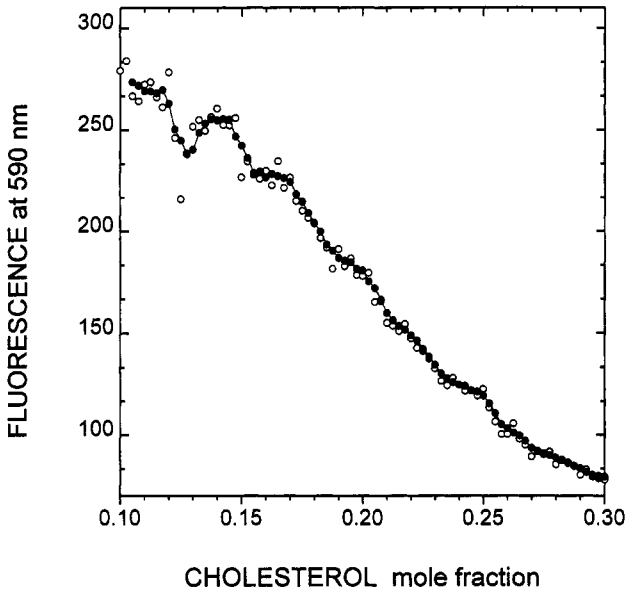

FIGURE 7: Binding of merocyanine 540 to DMPC–cholesterol liposomes as a function of cholesterol mole fraction. Binding of merocyanine to the liposomes was assessed from the fluorescence intensity at 590 nm, which also reflects the amount of merocyanine bound to the liposomes (see Experimental Procedures). The data points (open symbols) are averages from three parallel experiments, and the closed symbols represent four-point running averages. Deviations (dips or shoulders) are seen close to CMFs 0.12, 0.16, 0.20, and 0.25. Consistent results were obtained with samples prepared from other stock solutions with different data point intervals or with different concentrations of merocyanine 540 (not shown).

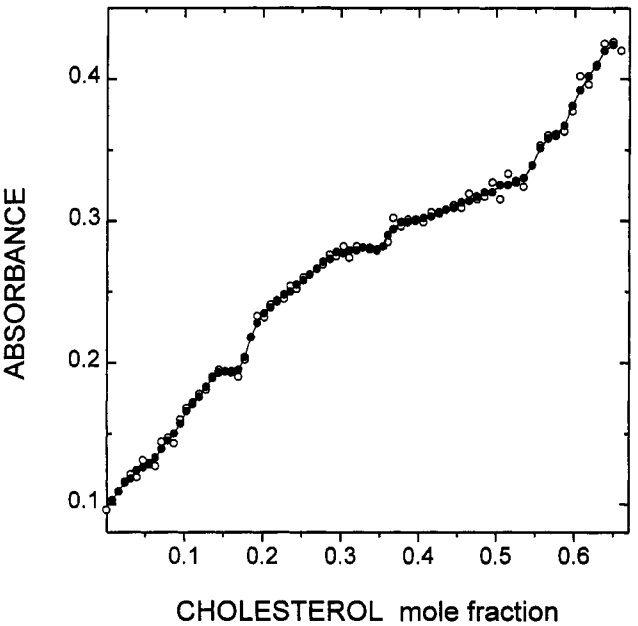

FIGURE 8: Absorbance (turbidity) of DMPC–cholesterol liposome suspensions as a function of cholesterol mole fraction. The data from four parallel experiments (open symbols) were averaged and plotted together with four-point running averages (closed symbols). Clear kinks or saturation-like phenomena are observed close to CMFs 0.16, 0.34, and 0.52. The data are compatible with the presence of kinks also at 0.20 and, possibly, at 0.40.

(turbidity) and light scattering beyond CMF 0.67 is probably due to the appearance of cholesterol microcrystals. Analysis of data scatter (not shown) supported the critical nature of the CMFs 0.15, 0.20, 0.33, and 0.50 in particular.

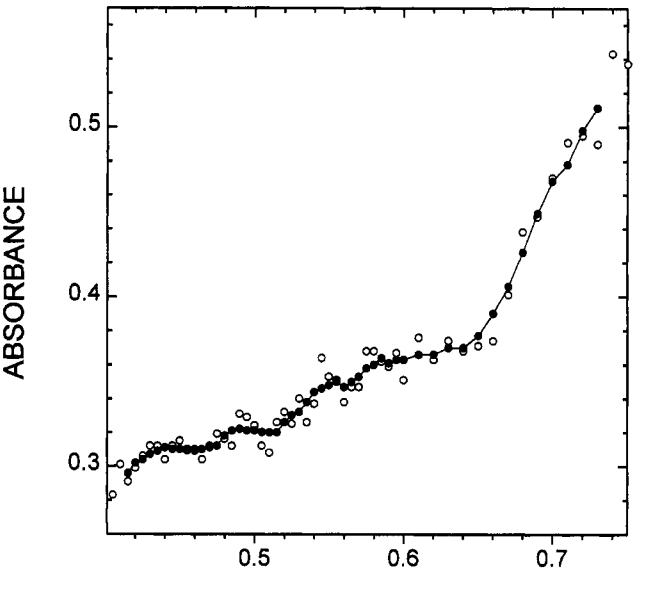

FIGURE 9: Absorbance (turbidity) of DMPC–cholesterol liposome suspensions as a function of cholesterol mole fraction. The data from two parallel experiments were averaged (open symbols) and plotted together with five-point running averages (closed symbols). An abrupt increase in sample turbidity takes place close to CMF 0.66, probably due to the presence of increasing amounts of cholesterol microcrystals. An abrupt increase in 90° light scattering close to CMF 0.66 was also observed (not shown).

We note that it is not straightforward to decide exactly which regions should be assigned to a critical CMFs in plots like those shown in Figures 8 and 9. This is because, to the best of our knowledge, no simple theory describing the relationship between bilayer lateral order and turbidity (light scattering) has been presented. We have chosen the point where an abrupt increase in the slope occurred after a plateau as the critical CMF. This choice is based on the fact that a shallow dip, albeit partially obscured by the smoothing procedure, frequently appeared to be present at those regions, particularly at CMFs 0.16 and 0.34 (cf. Figure 8). It seems feasible that such a local minimum in turbidity would correspond to a critical CMF, where the lateral homogeneity of the bilayer is maximal and, consequently, domain boundaries, probably contributing to the data scatter, are minimized, according the superlattice model (see the following).

DISCUSSION

Superlattice Domain Model for Phospholipid–Cholesterol Membranes. Collectively, the data shown above provide strong evidence that the physical properties of DMPC–cholesterol bilayers do not vary smoothly with cholesterol concentration, but undergo abrupt changes at certain (critical) CMFs, i.e., 0.12, 0.15, 0.20, 0.25, 0.33, 0.40, 0.50, and 0.67. The occurrence of critical events at these CMFs is most readily explained in terms of the superlattice (SL) model, which was developed previously to explain the lateral organization of pyrenyl lipids in bilayers (Somerharju et al., 1985; Virtanen et al., 1988) and is strongly supported by recent experimental and theoretical data (Tang & Chong, 1992; Chong et al., 1994; Sugar et al., 1994). The SL model, when applied to the cholesterol–phospholipid system, states the following: (i) phospholipid acyl chains exist in a lattice

with hexagonal (trigonal) symmetry; (ii) each cholesterol molecule replaces a single acyl chain in such a lattice; (iii) cholesterol molecules cause local lattice perturbations because of their larger cross-sectional area; (iv) the overall lattice perturbation (energy) is minimized when the cholesterol molecules are maximally separated from each other; and (v) such maximal (and equal) separation is realized when the cholesterol molecules form a superlattice with hexagonal or centered rectangular symmetry.

The predictions of the model are that (i) there is only a limited number of critical CMFs, each corresponding to a particular cholesterol superlattice, (ii) the overall lattice order obtains a maximum at each critical CMF, and (iii) two types of domains with two distinct cholesterol superlattices, as well as domains with random distribution, coexist at CMFs intermediate to the critical ones (Sugar et al., 1994). The critical mole fractions corresponding to hexagonal guest (cholesterol) superlattices are obtained from the following equation:

$$x_{HX} = \frac{2}{a^2 + ab + b^2 + 2 - f} \quad (1)$$

where a and b are the coordinates of the quest molecules closest to the one at the origin (Virtanen et al., 1988; cf. Figure 10). The parameter f is equal to the number of alkyl chains replaced by the guest in the lattice.

On the basis of the same principles, an equation that gives the critical mole fraction corresponding to centered rectangular superlattices was derived:

$$x_{CR} = \frac{2}{b^2 + 2ab + 2 - f} \quad (2)$$

The value of f may be estimated from the cross-sectional size of the guest relative to that of the alkyl chain. Alternatively, f may be obtained from eq 1 or 2, provided that an adequate number of critical guest mole fractions can be determined from the experimental data. Table 1 lists the critical cholesterol mole fractions calculated according to eqs 1 and 2 by assuming that each cholesterol replaces one acyl chain in the lattice (see the following). Comparison of the observed and predicted CMFs shows remarkably good agreement. The observed CMFs at 0.12, 0.15, 0.20, and 0.25 correspond to superlattices of hexagonal symmetry, while that at 0.33 corresponds to a centered rectangular cholesterol superlattice. Superlattices at CMFs 0.40 and 0.50 could have either centered rectangular or hexagonal symmetry (see the following). The critical CMF at 0.67 is not predicted directly by the SL model, but can be accounted for by assuming that, in this (limiting) case, cholesterol and DMPC molecules form alternating rows (see the following); this is equivalent to the formation of cholesterol superlattices of rectangular symmetry.

The SL model also predicts that the bilayer lateral order obtains a (local) maximum at the critical fractions (Sugar et al., 1994). Moving in either direction from a critical mole fraction should lead to a composition-driven order-to-disorder phase transition. Since fluctuations are maximal at the phase transition region (Hill, 1963), the increased data scatter (Figures 3B and 4) and intensity fluctuations (Figure 5) close to the critical CMFs support the occurrence of phase transitions in those regions. The abrupt change in the

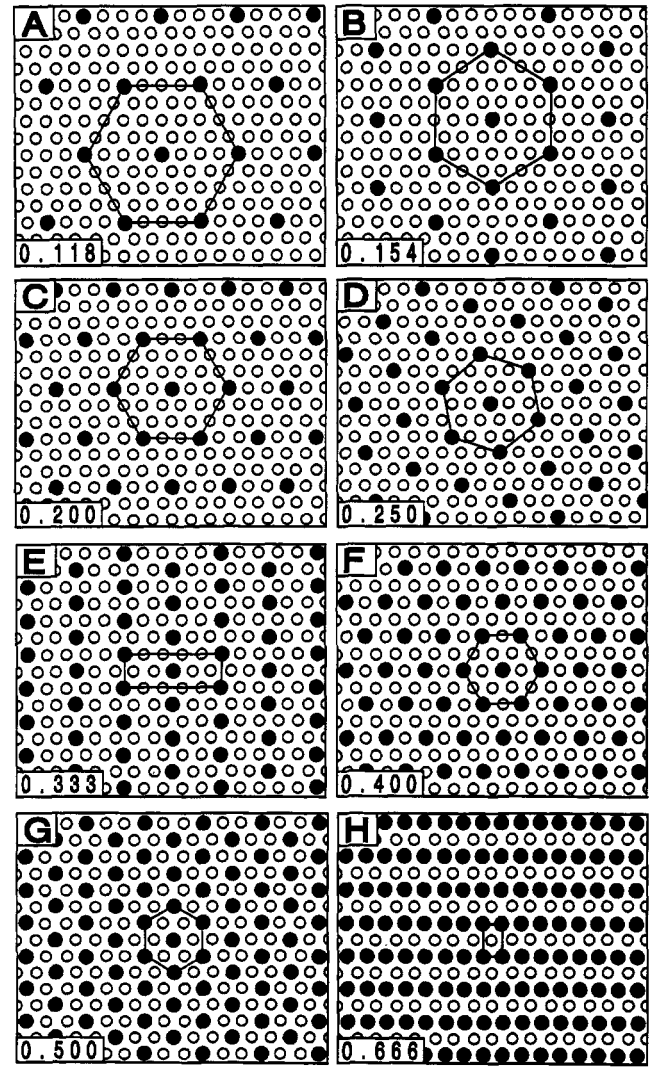

FIGURE 10: Structures of cholesterol superlattices corresponding to the observed critical cholesterol mole fractions according to the superlattice model. The acyl chains (open spheres) are assumed to form a hexagonal lattice where each cholesterol molecule (closed spheres) replaces a single acyl chain. Because the cholesterol molecules tend to maximize their distance from each other according to the model, cholesterol superlattices are formed. These superlattices are assumed to be local, minimum-energy structures that generally coexist with domains with a different superlattice, as well as with those having a more or less random distribution of the cholesterol molecules (see text). The critical cholesterol mole fraction corresponding to the superlattice is indicated in the lower left corner of each panel (A, 0.118; B, 0.154; C, 0.20; D, 0.25; E, 0.333; F, 0.40; G, 0.50; H, 0.666). The superlattice corresponding to CMF 0.333 (E) has a centered rectangular symmetry, that corresponding to CMF 0.666 (H) has a rectangular symmetry, and the rest have a hexagonal symmetry. See Table 1 for the corresponding lattice coordinates (a and b).

percolation frequency, which is associated with phase transitions (Snyder & Freire, 1980), could also contribute to the increased data scatter (Sugar et al., 1994). Conversely, the fluctuations should be minimal and the lateral homogeneity maximal at the critical CMFs, and thus the data scatter and intensity fluctuations should be minimal, as is generally observed. However, it is important to note that all regions of low data scatter should not be considered minima due to a coincident critical CMF. This is because, according to the superlattice model, regions of low (nonincreased) data scatter also occurs elsewhere, i.e., between the scatter peaks associated with two consecutive critical CMFs.

The correlation of the observed data scatter with domain fluctuations can be explained as follows. At those cholesterol concentrations (between two critical CMFs) where a transition from one to another type of domain takes place, a particularly heterogeneous (in terms of composition and/or size) population of liposomes could form due to enhanced bilayer fluctuations occurring at these regions and, conversely, this heterogeneity should reach a minimum at each critical CMF where a single domain type (superlattice) prevails. Thus, the heterogeneity of the liposomes would be a function of the lateral heterogeneity of the bilayers at the moment of dispersion. That the observed data scatter is indeed related to some property inherent to the liposomes rather than to errors in determining the fluorescence intensities is indicated by the fact that the scatter profiles remained largely unchanged when the same samples were measured again (data not shown). Supporting cholesterol concentration-dependent heterogeneity of the liposomes, short-term fluctuations in sample intensity follow a pattern similar to that of the data scatter, i.e., reached a local minimum at the same CMFs (Figure 5). Previously, Humphrey and Lovejoy (1983) provided evidence that the (size) heterogeneity of DMPC−cholesterol liposomes is dependent on CMF. In conclusion, the analyses of data scatter and short-term intensity fluctuations support the existence of composition-driven phase transitions between the critical CMFs and, consequently, the validity of the SL model.

Recently, Chong (1994) observed abrupt deviations (dips) in the fluorescence intensity of a cholesterol analogue, dehydroergosterol (DHE), in DMPC bilayers at DHE mole fractions very similar to the critical CMFs observed in this study. The results were interpreted in terms of a superlattice-like organization of the fluorescent sterol, and it was also suggested that cholesterol would be similarly distributed. Our present results strongly support this proposition. In the following, the critical CMF (superlattices) will be discussed in view of present and previous experimental evidence. Note that reference is made only to data obtained above T_m of the matrix phospholipid.

CMFs below 0.154. The SL model predicts a number of critical mole fractions occurring at CMF 0.143 and below (Table 1). While kinks, dips, or other deviations in the fluorescence parameter versus CMF plots and/or peaks of data scatter close to some of these predicted CMFs were frequently observed, most notably at CMF 0.118 (cf. Figures 2 and 7), these deviations could not be identified reproducibly. A similar lack of reproducibility in dips of DHE fluorescence below DHE mole fraction 0.154 was reported by Chong (1994), and it may be due to (i) instability (to thermal disruption) of the corresponding sterol superlattices, (ii) proximity of the neighboring critical CMFs, like those at 0.091 and 0.10 or 0.118 and 0.125 (Table 1), and/or (iii) increased data scatter that typically occurs close to the critical CMFs. Furthermore, we dispersed the lipids, for technical reasons (see Experimental Procedures), by a brief sonication that is expected to produce smaller liposomes with more curved bilayers than what would be obtained with vortex mixing, for instance. Data obtained for another, similar system show that such increased curvature tends to moderate the deviations occurring at the critical mole fractions, probably by destabilizing the guest superlattices (Sugar et al., 1994).

CMF 0.154. A deviation was observed persistently at this CMF by fluorescence and absorbance measurements (Figures 1B, 2, and 6−8). Very frequently, a scatter minimum with a proximal scatter peak(s) was observed close to this CMF, supporting its critical nature. The lateral organization of cholesterol at this mole fraction, as predicted by the SL model, is shown in Figure 10B. Supporting the critical nature of this CMF, a reproducible dip in the fluorescence intensity was observed at the corresponding DHE mole fraction (Chong, 1994). In addition, various other authors have shown, with different techniques, deviations in the CMF region 0.15−0.18 (Blok et al., 1977; Rubenstein et al., 1980; Alecio et al., 1982; Melchior et al., 1985; Wilcox et al., 1993; Kodati & Lafleur, 1993; Parasassi et al., 1994).

CMF 0.20. Several studies have indicated that critical events may occur at this CMF (Schwartz et al., 1976; Oldfield et al., 1978; Poznansky & Czekanski, 1979; Smith et al., 1980; Rubenstein et al., 1980; Melchior et al., 1980; Lenz et al., 1980; Chong, 1994). The present data are in accord with this (Figures 5−7). However, the deviations at this CMF were not as pronounced as those at 0.15 and 0.34, for instance. The superlattice corresponding to this CMF would have hexagonal symmetry, as shown in Figure 10C.

CMF 0.25. This is also a possible critical CMF according to the SL model. While we did not persistently observe a deviation at this CMF, the MC540 binding data (Figure 7) indicate that it may be a critical one. This is supported by an abrupt increase in data scatter that was frequently observed close to this CMF with each method (not shown). Chong (1994) found a marked dip in DHE fluorescence at a DHE mole fraction of 0.25 in DMPC.

CMF 0.33. A marked, reproducible deviation close to this CMF was detected with all approaches used in the present study (Figures 1B, 6, and 8), thus marking it as a critical one. This is supported by the analysis of data scatter (Figures 1C and 4) and time-dependent fluctuations (Figure 5). Many previous studies have provided evidence for critical events at CMF 0.30−0.34 (Lecuyer & Dervichian, 1969; Tsong, 1975; Newman & Huang, 1975; Blok et al., 1977; Tajima & Gersfeld; 1978; Poznansky & Czekanski, 1979; Rubenstein et al., 1980; Lenz et al., 1980; Melchior et al., 1980; Yin et al., 1987; Schroeder et al., 1987; Needham & Nunn, 1990; Linseisen et al., 1993; Parasassi et al., 1994). Importantly, several of these studies have demonstrated that a deviation at this CMF persists over a considerable temperature range above T_m (Brulet & McConnell, 1977; Rubenstein et al., 1980; Lenz et al., 1980), suggesting that the lateral arrangement of the components corresponding to this CMF is particularly stable (see the following). Interestingly, the superlattice corresponding to this CMF has a centered rectangular symmetry (Table 1 and Figure 10E) unlike those occurring at lower CMFs. This change in symmetry could relate to the (intrinsically) ellipsoidal horizontal cross section of the cholesterol molecule. At low cholesterol concentrations the axial rotation of cholesterol is rapid, so that its effective shape would be cylindrical, and thus there should not be any preferred lateral direction of interaction with the matrix. However, at high cholesterol concentrations the rotation of cholesterol molecules is probably slowed down, as indicated by the data of Shin and Freed (1989), with the result that the asymmetric cross-sectional shape of the cholesterol becomes "effective". This, in turn, would mean that the steric strain imposed on the acyl chain lattice by the

cholesterol molecules would become laterally anisotropic, thus favoring the adaptation of the less symmetric, centered rectangular superlattice arrangement. This change in packing symmetry would be analogous to the replacement of the hexagonal packing of an alkyl chain by rectangular packing upon slowing down of the axial rotation upon cooling (Small, 1984).

CMF 0.40. Although a minimum of data scatter or sample fluctuation was frequently observed at or close to this CMF (Figures 1D, 4, and 5), significant deviations in the measured parameter versus CMF plots were not observed persistently at this CMF. This could indicate that the corresponding superlattice is unstable, possibly because the arrangement of the cholesterol molecules in the superlattice could be energetically unfavorable. In agreement with this, little published data indicating critical events at this CMF appear to exist. Furthermore, as discussed earlier, low data scatter at a certain CMF does not necessarily mean that it is a critical one; such a minimum could be brought about simply by (coincidental) juxtaposition of two scatter peaks associated with two consequent critical CMFs (those at 0.33 and 0.50 in the present case). While the superlattice corresponding to CMF is depicted in Figure 10F as a hexagonal one for simplicity, it may actually have centered rectangular symmetry because of the asymmetric shape of the cholesterol molecules, as discussed earlier.

CMF 0.50. The critical nature of this CMF is indicated most clearly by the abrupt change in absorbance (turbidity) at this CMF (Figure 8). A marked increase in data scatter was also typically observed close to that CMF, as shown by Figures 1D, 3B, and 4. Yet the sample fluctuation (heterogeneity) data are compatible with this CMF being a critical one (Figure 5), and several previous studies have marked this CMF as a critical one (Lecuyer & Dervichian, 1969; Green & Green, 1973; Lenz et al., 1980; Ibdah & Phillips, 1988; Needham & Nunn, 1990; Mattjus & Slotte, 1994). The superlattice corresponding to this CMF is depicted in Figure 10G and, for the reasons mentioned earlier, may actually have centered rectangular symmetry instead of the depicted hexagonal.

CMF 0.67. As shown by the *E/M* and absorbance data, saturation of the cholesterol-induced change in bilayer properties is clearly observed close to a CMF of 0.67 (Figures 1A,C, 3A, and 9), suggesting that this CMF (cholesterol/PL = 2/1) corresponds the maximum solubility of cholesterol in DMPC bilayers. Previously, several groups have demonstrated that PC vesicles or liposomes can incorporate cholesterol up to a 2/1 cholesterol/PL molar ratio (Horwitz et al., 1971; Freeman & Finean, 1975; Reiber, 1978; Lundberg, 1977; Green & Green, 1973). On the other hand, there are studies indicating that cholesterol can be accommodated only up to a 1/1 molar ratio (Landbrooke et al., 1969; Lecuyer & Dervichian, 1969). This discrepancy can be explained as follows. In those cases where 2/1 stoichiometry has been observed, unilamellar vesicles were usually employed, while multilamellar dispersion was used when a 1/1 limiting ratio has been observed. This suggests that apposition of bilayers, which is obviously more feasible in multilamellar aggregates than in unilamellar vesicles, plays a central role in determining the stability of bilayers at high cholesterol/PL ratios. Supporting this, McIntosh et al. (1989) have shown that the addition of cholesterol to egg PC bilayers decreases interbilayer separation under high pressures. In line with this, the thickness of the aqueous layer separating the bilayers decreases markedly at high (>0.33) cholesterol mole fractions (Lecuyer & Dervichian, 1969). Therefore, it is likely that destabilization due to intermembrane contacts, rather than limited (two-dimensional) solubility of cholesterol, is responsible for the maximal 1/1 stoichiometry frequently observed for multilamellar dispersion. Supporting this, red cell suspensions, where interbilayer contacts are prevented by the membrane proteins, can incorporate cholesterol up to CMF 0.67 (Cooper et al., 1978). Furthermore, in PC monolayers cholesterol-induced condensation increases steadily up to CMF 0.67, after which no additional condensation is observed (Lundberg, 1982). The proposed lateral organization of DMPC–cholesterol bilayers at CMF 0.67 is depicted in Figure 10H. The corresponding cholesterol superlattice differs from those at lower CMFs in that it has neither hexagonal nor centered rectangular symmetry, but a rectangular symmetry.

Forces Involved in the Formation of Cholesterol Superlattices. At CMFs of 0.25 and above, all acyl chains can simultaneously interact with cholesterol (see Figure 10D), and nearest neighbor interactions could explain the formation of cholesterol superlattices (or "compounds"). Thus, there is no need to invoke long-range lattice forces at high CMFs. However, such forces would be needed to maintain cholesterol superlattices at lower CMFs. Previously we suggested, to explain the formation of PyrPC superlattices, that steric strain imposed on the acyl chain lattice by the bulky pyrenyl moiety plays a major role (Somerharju et al., 1985). Because cholesterol is also much bulkier than an (condensed) acyl chain, steric strain could also operate in the present case. However, for the steric strain to extend beyond the proximal acyl chains, packing of the components close to the van der Waals distances is required. There is considerable evidence for such a close packing in cholesterol-containing membranes, as best demonstrated by data on cholesterol–phosphatidylcholine monolayers (de Bernard, 1958; Shah & Schulman, 1967; Lecuyer & Dervichian, 1969; Lundberg, 1982; also see the following). In Figure 11 the surface area per acyl chain is plotted as the function of cholesterol mole fraction in egg PC monolayers. As can be seen, the area per chain decreases considerably with cholesterol concentration and approaches 20 Å^2 at CMF 0.50. This value is very similar to those of hexagonally packed, crystalline hydrocarbons (Small, 1984), thus showing that close packing of the components can indeed exist in cholesterol–PC membranes. In line with this, NMR and IR data show remarkable conformational ordering of lipid acyl chains by cholesterol (Seelig & Seelig, 1980; Davies et al., 1990; Sankaram & Thompson 1990; Cheng et al., 1994), and the rate of lipid lateral diffusion decreases several-fold upon the addition of 50 mol % cholesterol to DMPC bilyers (Smith et al., 1980; Shin & Freed, 1989). It should also be noted that, even at the relatively low CMF of 0.118, none of the acyl chains is more than two lattice sites away from a cholesterol molecule (Figure 10A) and thus are very likely to "feel" the ordering effect of the cholesterol molecules, as also indicated by recent molecular dynamics simulations (Edholm & Nyberg, 1992). Thus, cholesterol-induced perturbation does not have to extend over long distances to produce superlattices, even at relatively low CMFs. However, as the (overall) ordering effect of cholesterol decreases with its mole fraction, the superlattices become progressively more prone to thermal

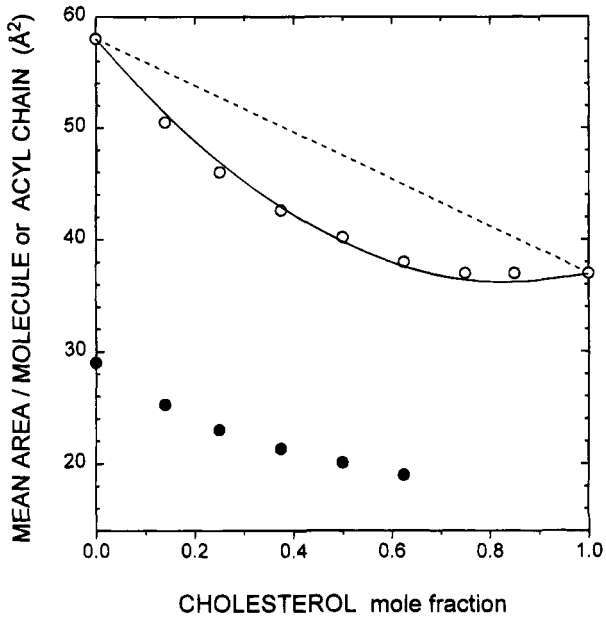

FIGURE 11: Mean area per molecule or acyl chain versus cholesterol mole fraction. The open symbols give the expertimentally determined mean area per molecule in egg PC–cholesterol monolayers (Lundberg, 1982) as a function of CMF. The continuous line represents the mean area per molecule obtained by fitting eq A3 (Appendix) to the experimental data, assuming that each cholesterol replaces a single acyl chain in the lattice as proposed by the SL model. The dashed line indicates the mean area per molecule in the case of ideal mixing, i.e., when no condensation occurs. The closed symbols indicate the area per alkyl chain, calculated from the (experimental) mean area per molecule with the assumption that the surface area of cholesterol remains constant at 37 Å^2 (see the Appendix).

disruption and, thus, cover less and less of the total membrane area (see the following).

In neat, liquid-crystalline bilayers, packing of the phosphatidylcholine molecules is constrained by the head-group, which has a larger surface area than the hydrophobic part of the molecule (McIntosh, 1980; Presti et al., 1982). Supporting this, the addition of cholesterol significantly enhances the mobility of PC head-groups, probably by acting as a spacer at the head-group level (Oldfield et al., 1978). This energetically favorable spacer effect is expected to be maximal when the cholesterol molecules distribute in a regular fashion in the plane of the bilayer and, consequently, could contribute to the formation of cholesterol superlattices. As an example of the organizing effect of spacer molecules, Bucher and Kuhn have shown that, in monolayers of dialkylcyanine dyes, which have a large head-group relative to the alkyl chains, a remarkable increase in lateral order takes place when octadecane is added to reach a 1/1 molar ratio. Octadecane molecules were suggested to intercalate between the dye molecules, thus allowing close packing of the alkyl chains, otherwise inhibited by the bulky head-groups. A centered, rectangular superlattice of the dye molecules was proposed to be formed (Bucher & Kuhn, 1970).

SL Model and the Condensing Effect of Cholesterol. It is well-established that cholesterol can induce marked condensation (i.e., decrease in mean area per molecule) of liquid-crystalline phosphatidylcholine bilayers (de Bernard, 1958; Lecuyer & Dervichian, 1969). Obviously, any model of lateral arrangement of cholesterol–phosphatidylcholine bilayers should adequately account for this condensing effect. A basic feature of the present SL model is that each cholesterol molecule replaces a single acyl chain in the lattice. Importantly, it appears that the condensing effect of cholesterol can be readily accounted for by this presumption, but not if the replacement of two acyl chains, for instance, by each cholesterol molecule is postulated (see the following). This can be readily demonstrated by examining data published on PC–cholesterol monolayers. Egg PC rather than DMPC monolayers are referred to here because most detailed data are available on this phospholipid (de Bernard, 1958; Lundberg, 1982), and because the interpretation of the data is not complicated by the proximity of the critical temperature. However, the condensing effect of cholesterol in DMPC monolayers has been stated to be very similar to that observed for egg PC (Subramaniam & McConnell, 1987). It is also relevant to note that there is close analogy in the behavior of mono- and bilayers (MacDonald & Simon, 1987; Vaknin et al., 1991).

The (limiting) surface areas for egg PC and cholesterol molecules are approximately 58 (i.e., 29 Å^2 per an alkyl chain) and 37 Å^2, respectively (Lecuyer & Dervichian, 1969; Lundberg, 1982). If two acyl chains, i.e., a whole phospholipid molecule, were replaced by each cholesterol in the lattice, no decrease in the mean area per molecule would occur, since the surface area of cholesterol is much smaller than that of an egg PC molecule. In fact, the average area should increase because the chains proximal to the added cholesterol molecules should expand in order to fill the void corresponding to the area difference. Thus, it is obvious that the replacement of a whole phospholipid molecule (two acyl chains) by cholesterol cannot bring about any condensation. However, such condensation (i.e., decrease in mean area per molecule) would occur if cholesterol replaces only one acyl chain in the lattice. To demonstrate this, it is instructive to calculate first how much the proximal acyl chains should condense to accommodate a cholesterol molecule in a lattice site under the (hypothetical) condition that the lattice area remains constant. At low and moderate cholesterol concentrations, when each cholesterol is surrounded only by unshared acyl chains, the proximal chains together should give up 8 Å^2 (37–29 Å^2) to accommodate one cholesterol molecule to maintain constant lattice area. Since a host lattice with hexagonal symmetry is assumed (Ruocco & Shipley, 1982), the added cholesterol molecule would be surrounded by six acyl chains and each of these chains should give up 1.33 Å^2 of their original surface area. Thus, a minor (4.6%) condensation of each proximal acyl chain is required to accommodate cholesterol molecules to maintain a constant lattice area. Since those acyl chains that are not in direct contact with cholesterol are probably also affected by cholesterol (Edholm & Nyberg, 1992), albeit by less than the proximal ones, the latter need to condense even less than indicated by the preceding figure. Accordingly, it is obvious that a cholesterol molecule, despite its considerably larger surface area, can be readily accommodated in the acyl chain lattice without expansion of the latter.

To fully account for the observed condensing effect of cholesterol, the lattice area should actually decrease rather than remain constant. To model this, we derived a formula (see Appendix) on the basis of the assumption that acyl chain condensation is a linear function of cholesterol mole fraction (Lundberg, 1982). As shown by Figure 11, this simple

formula can predict well the condensation of egg PC monolayers by cholesterol, strongly suggesting that one of the basic assumptions of the SL models, i.e., that each cholesterol replaces a single acyl chain, is indeed valid. We note that this conclusion is also consistent with a more detailed quantitative analysis of the cholesterol-induced condensation (unpublished data).

To account for a dip in DHE fluorescence at DHE mole fraction 0.33, Chong (1994), deviating from our interpretation, recently proposed that at this mole fraction and above DHE (and, thus, presumably also cholesterol) replaces two acyl chains rather than one in the lattice. If this were the case, the cholesterol-induced condensation should be abolished at or close to this mole fraction (see above). However, experimental data do not show the disappearance or abrupt decrease in the condensing effect around this CMF; rather, this effect is maintained to much higher CMFs (de Bernard, 1958; Shah & Schulman, 1967; Lundberg, 1982). Therefore, we feel that the discontinuity (dip) observed at CMF 0.33 is better explained by assuming that cholesterol still replaces one acyl chain, but adopts a centered rectangular, rather than a hexagonal distribution (cf. Figure 10E). Notably, Chong's interpretation was based on a surface area of 26.7 Å^2 for cholesterol, which is far below the value of 37−38 Å^2 obtained with the monolayer method (de Bernard, 1958; Lundberg, 1982), by X-ray analysis of cholesterol−phosphatidylcholine bilayers (Lecuyer & Dervichian, 1969), or as estimated from the crystal structure (Hsu & Nordman, 1983).

Compatibility of the SL Model with Published Cholesterol−Phospholipid Phase Diagrams. Many cholesterol−phosphatidylcholine phase diagrams have been published (Lenz et al., 1980; Rectenwald & McConnel, 1981; Ipsen et al., 1987; Vist & Davies, 1990; Sankaram & Thompson, 1990; McMullen et al., 1994). Generally, these phase diagrams allow for two distinct phases above the gel-to-liquid transition temperature, i.e., the liquid-disordered (l_d) and the liquid-ordered (l_o) phases, which are separated by a coexistence ($l_d - l_o$) region (Ipsen et al., 1987). No particular lateral arrangement of the components in those phases is assumed. The present data, indicating that several sequential transitions from one type of lateral arrangement of cholesterol to another occur with increasing CMF, suggest that revision of the cholesterol−phosphatidylcholine phase diagram is required.

Supporting the SL model, several authors have provided evidence for vertical "phase" boundaries above T_m, i.e., critical CMFs do not shift significantly with temperature. This has been most clearly demonstrated for CMF 0.33 (Brulet & McConnell, 1977; Rubenstein et al., 1980; Lenz et al., 1980). Also, for the analogous PyrPC/DMPC system, the mole fractions at which the critical events were observed were found be temperature-independent (Chong et al., 1994). The magnitude of the deviations (dips or kinks), however, decreased with temperature, indicating that the lateral organization (i.e., superlattices) is, as expected, sensitive to thermal disruption. Such temperature-dependent conversion of the superlattice domains to randomly organized ones would also explain why sloping of the phase boundaries toward higher CMFs appears to occur (Sankaram & Thompson, 1990). Other factors that may also contribute to the observed sloping of the boundaries are (i) the rapid exchange of molecules between distinct domains, (ii) the small size and short lifetime of the domains (Mouritsen & Biltonen, 1993), and (iii) the long characteristic time of the method (NMR, ESR) used to determine the boundaries. The problems with relating microscopic membrane domains to macroscopic phases have been discussed by Rectenwald and McConnell (1981).

The lateral organization of cholesterol below the gel-to-liquid phase transition temperature (T_m) of DMPC was not studied here, but there is no reason a priori to assume that the organization of cholesterol in superlattices would not also take place below T_m. On the contrary, the higher ordering of the bilayers below T_m should actually enhance the steric strain that cholesterol molecules impose on the acyl chain lattice and, consequently, the tendency of cholesterol to adopt regular, superlattice-like arrangements. Supporting this, a variety of previous studies have indicated changes in the bilayer properties close to the critical CMFs 0.20, 0.33, and 0.50 (Rubenstein et al., 1979; Rothman & Engelman, 1972; Mabrey & Sturtevant 1968; Estep et al., 1978) below T_m of the phospholipid. The recent calorimetric study of McMullen et al. (1993) on cholesterol−DMPC bilayers actually shows stepwise increments in the width of the broad component of the main transition close to CMF 0.15, 0.25, and 0.35, as is predicted by the SL model.

While the good agreement between the predicted and observed critical CMFs strongly supports the proposed superlattice model, there may be other explanations for the occurrence of critical events at the various CMFs observed here, or previously by other investigators. However, for any model to explain the critical CMFs, some kind of lateral regularity has to be invoked. We have considered several alternatives. For instance, one could assume that cholesterol forms trimers that are regularly distributed. While such a model is compatible with the critical CMFs observed here, it predicts many additional ones that were not observed. The same applies to models that include other types of cholesterol oligomers or cholesterol−phospholipid complexes. Furthermore, the strong condensing effect of cholesterol (Figure 11) is difficult to explain if clustering of cholesterol molecules is assumed. Actually, there is experimental evidence that cholesterol does not form dimers or other types of clusters in liquid-crystalline bilayers (Hyslop et al., 1990). The superlattice structures implicated by the present data could be observable by X-ray or neutron diffraction studies. However, a synchrotron X-ray source may be needed, because the superlattice domains are probably limited in size and relatively short-lived in the liquid-crystalline state studied here.

We note that, after this manuscript was submitted to publication, two independent studies appeared wherein evidence for the regular distribution of cholesterol in DMPC bilayers was obtained (Tang et al., 1995; Parasassi et al., 1995).

Biological Implications of Cholesterol-Driven Domain Segregation. Previous studies have shown that minor changes in membrane cholesterol content can cause marked changes in the activity of membrane-associated enzymes [reviewed by Yeagle (1991)]. In particular, Connolly et al. (1985) showed that increasing CMF from 0.10 to 0.125 in fluid dipalmitoylphosphatidylcholine bilayers caused a 100-fold decrease in the activity of the reconstituted hexose transporter of human erythrocytes. Equally strikingly, the activity was restored to the initial level upon further increase of CMF to 0.20! Such reversible, cholesterol concentration-

dependent changes in enzyme activity could result from abrupt changes in the lateral order of the lipid matrix, as predicted by the SL model, leading, for instance, to massive aggregation and, thus, inactivation of the transporter molecules. Abrupt cholesterol concentration-dependent changes in the activity of rat hepatic lipase acting on lipid monolayers have also been noted, and these correlated with changes in lipid packing (Wilcox et al., 1993).

Recently, Bretscher and Munro (1993) proposed that the increase in cholesterol concentration in the Golgi membranes causes the segregation of domains with high and low cholesterol concentrations, respectively. Since the high-cholesterol domains are considerably thicker than those with low cholesterol concentrations (Levine & Wilkins, 1971; Nezil & Bloom, 1992), integral membrane proteins were suggested to partition between the domains according the length of their transmembrane segments. The Golgi-specific proteins generally have considerably shorter transmembrane segments than those found in the plasma membrane (Bretcher & Munro, 1993); thus, they could preferentially partition to low-cholesterol (thinner) domains, while the plasma membrane proteins should prefer the high-cholesterol (thicker) domains. Subsequent segregation of the low- and high-cholesterol domains along the secretory pathway would then accomplish sorting of the plasma membrane proteins from those to remain in the Golgi. While these authors propose only two different types of domains, the present data, as well as that by Chong (1994), strongly suggest that with increasing cholesterol concentrations multiple composition-driven "phase" transitions are encountered, each separating two phases with different cholesterol concentrations. This would be equal to the occurrence of multiple partition steps, which could result in considerable enhancement of membrane protein segregation based on structure-dependent partition between domains with distinct cholesterol concentrations.

Segregation into domains having distinct cholesterol concentrations obviously could play an important role in the intracellular transport and sorting of cholesterol (Bretcher & Munro, 1993) and of sphingomyelin since the latter lipid appears to specifically associate with cholesterol in cells (Lange et al., 1989). Yet, it is of interest to note that both experimental data (Käs & Sackmann, 1991) and theoretical studies (Lipowsky, 1993) indicate that domain segregation can lead to the spontaneous budding of vesicles from lipid bilayers. This suggests that domain segregation could be a crucial step in the budding of vesicles carrying lipids and proteins from the internal membranes to the plasma membrane and vice versa (Lipowsky, 1993).

ACKNOWLEDGMENT

The expert technical assistance of Ms. Tarja Grundström, Ms. Mervi Toivari, Ms. Terhi Kärpänen, and Mr. Kimmo Tanhuanpää is gratefully acknowledged. We are also indebted to Drs. Kwan Hon Cheng and Massimo Sassaroli for critical reading of the manuscript and to Drs. Istvan Sugar and Gerald Huth for helpful discussions.

APPENDIX

If cholesterol and a phospholipid were to mix ideally in a mono- or bilayer, the mean molecular area (A_{ideal}) would be given by the following equation:

$$A_{ideal} = xA_{Chol} + (1 - x)A_{PL} \quad \text{(A1)}$$

where A_{Chol} and A_{PL} are the areas per molecule for cholesterol and phosholipid, respectively, and x is the cholesterol mole fraction. Generally, however, the mixing is not ideal, as indicated by a negative deviation from the linear dependency predicted by eq A1 (de Bernard, 1958). This negative deviation is due to condensation of the acyl chains by the rigid cholesterol molecules (see Discussion). As indicated by the data of Lundberg (1982), the condensation is a linear function of cholesterol mole fraction:

$$A_{alk} = (1 - Cx)A_{o,alk} \quad \text{(A2)}$$

where A_{alk} and $A_{o,alk}$ are the condensed and original areas for an acyl chain, respectively, and C is a proportionality (i.e., condensation) constant. By noting that $A_{PL} = 2A_{alk}$, substitution into eq A1 gives

$$A_{av} = xA_{Chol} + 2(1 - x)(1 - Cx)A_{o,alk} \quad \text{(A3)}$$

where A_{av} is the average (mean) area per molecule. The best fit (see Figure 11) to the experimental data is obtained when $C = 0.53$. See the Discussion for further details.

REFERENCES

Alecio, M. R., Golan, D. E., Veatch, W. R., & Rando, R. R. (1982) *Proc. Natl. Acad. Sci. U.S.A. 79*, 5171−5174.
Bloch, K. (1985) *Biochemistry of Lipids and Membranes* (Vance, D. E., & Vance, J. E., Eds.) pp 1−24, The Benjamin/Cummins Publishing Company, Inc., Menlo Park, CA.
Blok, M. C., van Deenen, L. L. M., & De Gier, J. (1977) *Biochim. Biophys. Acta 464*, 509−518.
Bretscher, M. S., & Munro, S. (1993) *Science 261*, 1280−1281.
Brulet, P., & McConnell, H. M. (1977) *Biochemistry 16*, 1209−1217.
Bucher, H., & Kuhn, H. (1970) *Chem. Phys. Lett. 6*, 183−185.
Burack, W. R., & Biltonen, R. L. (1994) *Chem. Phys. Lipids 73*, 209−222.
Carruthers, A., & Melchior, D. L. (1986) *Trends Biochem. Sci. 11*, 331−335.
Cheng, K. H., Ruymgaart, L., Liu, L., Somerharju, P., & Sugar, I. P. (1994) *Biophys. J. 67*, 902−913.
Chong, P. L.-G. (1994) *Proc. Natl. Acad. Sci. U.S.A. 91*, 10069−10073.
Chong, P. L.-G., Tang, D., & Sugar, I. P. (1994) *Biophys. J. 66*, 2029−2038.
Conolly, T. J., Carruthers, A., & Melchior,, D. L. (1985) *Biochemistry 24*, 2865−2873.
Cooper, R. A., Leslie, M. H., Fischoff, S., Shinitzky, M., & Shattil, S. J. (1978) *Biochemistry 17*, 327−331.
Davies, M. A., Schustet, H. F., Brauner, J. W., & Mendelsohn, R. (1990) *Biochemistry 29*, 4368−4373.
de Bernard, L. (1958) *Bull. Soc. Chim. Biol. 40*, 161−170.
Edholm, O., & Nyberg, A. M. (1992) *Biophys. J. 63*, 1081−1089.
Eklund, K., Virtanen, J. A., Kinnunen, P. K. J., Kasurinen, J., & Somerharju, P. (1992) *Biochemistry 31*, 8560−8565.
El-Sayed, M.-Y., Guion, T. A., & Fayer, M. D. (1986) *Biochemistry 25*, 4825−4832.
Engelman, D. M., & Rothman, J. E. (1972) *J. Biol. Chem. 247*, 3694−3697.
Estep, T. N., Mountcastle, D. B., Biltonen, R. L., & Thompson, T. E. (1978) *Biochemistry 17*, 1984−1989.
Freeman, R., & Finean, J. B. (1975) *Chem. Phys. Lipids 14*, 313−320.
Green, J. R., & Green, C. (1973) *Trans. Biochem. Soc. 1*, 365−367.
Hill, T. L. (1963) *Thermodynamics of Small Systems*, Benjamin, New York.
Horwitz, C., Krut, L., & Kaminsky, L. S. (1971) *Biochim. Biophys. Acta 239*, 329−336.

Hsu, L.-Y., & Nordman, C. E. (1983) *Science 220*, 604−606.
Huang, C.-H., Sipe, J. P., Chow, S. T., & Martin, R. B. (1974) *Proc. Natl. Acad. Sci. U.S.A. 71*, 359−362.
Humphries, G. M. K., & Lovejoy, J. P. (1983) *Biochem. Biophys. Res. Commun. 111*, 768−774.
Hyslop, P. A., Morel, B., & Sauerheber, R. D. (1990) *Biochemistry 29*, 1025−1038.
Ibdah, J. A., & Phillips, M. C. (1988) *Biochemistry 27*, 7155−7162.
Ipsen, J. H., Karlström, G., Mouritsen, O. G., Wennerström, H., & Zuckermann, M. J. (1987) *Biochim. Biophys. Acta 905*, 162−172.
Käs, J., & Sackmann, E. (1991) *Biophys. J. 60*, 835−844.
Kodati, V. R., & Lafleur, M. (1993) *Biophys. J. 64*, 163−170.
Landbrooke, B. D., Williams, R. M., & Chapman, D. (1968) *Biochim. Biophys. Acta 150*, 333−340.
Lange, Y., & Steck, T. L. (1994) *J. Biol. Chem. 269*, 29371−29374.
Lange, Y., Swaisgood, M. H., Ramos, B. V., & Steck, T. L. (1989) *J. Biol. Chem. 264*, 3786−3793.
Lecuyer, H., & Dervichian, D. G. (1969) *J. Mol. Biol. 45*, 39−57.
Lentz, B. R., Barrow, D. A., & Hoechli, M. (1980) *Biochemistry 19*, 1943−1954.
Levine, Y. K., & Wilkins, M. H. F. (1971) *Nature New Biol. 230*, 69−71.
Linseisen, F. M., Thewalt, J. L., Bloom, M., & Bayerl, T. M. (1993) *Chem. Phys. Lipids 65*, 141−149.
Lipowsky, R. (1993) *Biophys. J. 64*, 1133−1138.
Lundberg, B. (1977) *Chem. Phys. Lipids 18*, 212−220.
Lundberg, B. (1982) *Chem. Phys. Lipids 31*, 23−32.
Mabrey, S., & Sturtevant, J. M. (1976) *Proc. Natl. Acad. Sci. U.S.A. 73*, 3862−3866.
MacDonald, R., & Simon, S. A. (1987) *Proc. Natl. Acad. Sci. U.S.A. 84*, 4089−4093.
Martin, R. B., & Yeagle, P. L. (1978) *Lipids 13*, 594−597.
Mattjus, P., & Slotte, J. P. (1994) *Chem. Phys. Lipids 71*, 73−81.
McIntosh, T. J. (1980) *Biophys. J. 29*, 237−246.
McIntosh, T. J., Magid, A. D., & Simon, S. A. (1989) *Biochemistry 28*, 17−25.
McMullen, T. P. W., Lewis, R. N. A. H., & McElhaney, R. N. (1993) *Biochemistry 32*, 516−522.
Melchior, D. L., Scavitto, F. J., & Steim, J. M. (1980) *Biochemistry 19*, 4828−4834.
Melchior, T. J., Carruthers, A., & Melchior, D. L. (1985) *Biochemistry 24*, 2865−2873.
Mendelsohn, R., Davies, M. A., Schuster, H. F., Xu, Z., & Bittman, R. (1991) *Biochemistry 30*, 8558−8563.
Mouritzen, O. G., & Biltonen, R. L. (1993) in *Protein-Lipid Interactions* (Watts, A., Ed.) pp 1−39, Elsevier, Amsterdam.
Needham, D., & Nunn, R. S. (1990) *Biophys. J. 58*, 997−1009.
Newman, G. C., & Huang, C.-h. (1975) *Biochemistry 15*, 3363−3370.
Nezil, F. A., & Bloom., M. (1992) *Biophys. J. 61*, 1176−1182.
Oldfield, E., Meadows, M., Rice, D., & Jacobs, R. (1978) *Biochemistry 17*, 2727−2740.
Parasassi, T., Di Stefano, M., Loiero, N., Ravagnan, G., & Gratton, E. (1994) *Biophys. J. 66*, 763−768.
Parasassi, T., Giusti, A. M., Raimondi, M., & Gratton, E. (1995) *Biophys. J. 68*, 1895−1902.
Poznansky, M. J., & Czekanski, S. (1979) *Biochem. J. 177*, 989−991.
Presti, F. T., Pace, R. J., & Chan, S. I. (1982) *Biochemistry 21*, 3831−3835.
Rectenwald, D. J., & McConnell, H. M. (1981) *Biochemistry 20*, 4505−4510.
Reiber, H. (1978) *Biochim. Biophys. Acta 512*, 72−83.
Rubenstein, J. L. R., Smith, B. A., & McConnell, H. M. (1979) *Proc. Natl. Acad. Sci. U.S.A. 76*, 15−18.
Rubenstein, J. L. R., Owicki, J. C., & McConnell, H. M. (1980) *Biochemistry 19*, 569−573.
Ruocco, M. J., & Shipley, G. G. (1982) *Biochim. Biophys. Acta 691*, 309−320.
Sankaram, M. B., & Thompson, T. E. (1990) *Biochemistry 29*, 10676−10684.
Sankaram, M. B., & Thompson, T. E. (1991) *Proc. Natl. Acad. Sci. U.S.A. 88*, 8686−8690.
Sassaroli, M., Ruonala, M., Virtanen, J. A., Vauhkonen, M., & Somerharju, P. (1995) *Biochemistry 34*, 8843−8851.
Schroeder, F., Barenholtz, Y., Gratton, E., & Thompson, T. E. (1987) *Biochemistry 26*, 2441−2448.
Schwartz, F. T., Paltauf, F., & Laggner, P. (1976) *Chem. Phys. Lipids 17*, 423−434.
Seelig, J., & Seelig, A. (1980) *Q. Rev. Biophys. 13*, 19−61.
Shah, D. O., & Schulman, J. H. (1967) *J. Lipid Res. 8*, 215−226.
Shin, Y.-K., & Freed, J. H. (1989) *Biophys. J. 55*, 537−550.
Small, D. M. (1984) *J. Lipid Res. 25*, 1490−1500.
Smith, L. M., Rubenstein, J. L. R., Parce, J. W., & McConnell, H. M. (1980) *Biochemistry 19*, 5907−5911.
Snyder, B., & Freire, E. (1980) *Proc. Natl. Acad. Sci. U.S.A. 77*, 4055−4059.
Somerharju, P., Virtanen, J. A., Eklund, K. K., Vainio, P., & Kinnunen, P. K. J. (1985) *Biochemistry 24*, 2773−2781.
Subramaniam, S., & McConnell, H. M. (1987) *J. Phys. Chem. 91*, 1715−1718.
Sugar, I. P., Tang, D., & Chong, P. G.-L. (1994) *J. Phys. Chem. 98*, 7201−7210.
Tajima, K., & Gershfetd, N. L. (1978) *Biophys. J. 22*, 489−500.
Tang, D., & Chong. P. G.-L. (1992) *Biophys. J. 63*, 903−910.
Tang, D., Van Der Meer, W., & Chen, S.-Y. S. (1995) *Biophys. J. 68*, 1944−1951.
Tsong, T. Y. (1975) *Biochemistry 14*, 5415−5417.
Vaknin, D., Kjaer, K., Als-Nielsen, J., & Lösche, M. (1991) *Biophys. J. 59*, 1325−1332.
Verkman, A. S. (1987) *Biochemistry 26*, 4050−4056.
Virtanen, J. A., Somerharju, P., & Kinnunen, P. K. J. (1988) *J. Mol. Electron. 4*, 233−236.
Vist, M. R., & Davis, J. H. (1990) *Biochemistry 29*, 451−464.
Wilcox, R. W., Thuren, T., Sisson, P., Schmitt, J. D., Kennedy, M., & Waite, M. (1993) *Biochemistry, 32*, 5752−5758.
Williamson, P., Mattocks, K., & Schlegel, R. A. (1983) *Biochim. Biophys. Acta 732*, 387−393.
Yeagle, P. L. (1985) *Biochim. Biophys. Acta 822*, 267−287.
Yeagle, P. L. (1991) *Biochimie 73*, 1303−1310.
Yi, P. N., & MacDonald, R. (1973) *Chem. Phys. Lipids 11*, 114−134.
Yin, J.-J., Feix, J. B., & Hyde, J. S. (1987) *Biophys. J. 52*, 1031−1038.

BI9504769